Kartik Prasad[a], Vikas Kumar[a], Kota Bhanu Sankara Rao[b], Mahadevan Sundararaman[c]
[a] Defence Metallurgical Research Laboratory, Kanchanbagh, Hyderabad, India
[b] Ministry of steel chair professor, Mahatma Gandhi Institute of Technology, Hyderabad, India
[c] Department of Metallurgical and Materials Engineering, Indian Institute of Technology Madras, Chennai, India

Effects of silicon on characteristics of dynamic strain aging in a near-α titanium alloy

The effects of temperature and strain rate on the tensile properties of Timetal 834 near-α titanium alloy and alloy 834 without silicon were examined in the temperature range of 250 °C to 600 °C, employing strain rates in the range of 6.67×10^{-6} s^{-1} to 6.67×10^{-3} s^{-1}. Manifestations of dynamic strain aging such as serrated flow, plateaus in the variations of 0.2 % yield strength and ultimate tensile strength, peak in strain hardening exponent with temperature and negative strain rate sensitivity were observed in both the alloys. Serration maps in terms of strain rate versus temperature are presented for both the alloys. The activation energy for serrated flow was determined in both the alloys by employing various methodologies mentioned in the literature. Analysis of the results suggested that addition of Si leads to increased severity of dynamic strain aging.

Keywords: Dynamic strain aging; Titanium alloy; Tensile behavior; Activation energy; Serrated flow

1. Introduction

Timetal 834, a near-α titanium alloy containing less than 2 wt.% β stabilizing elements is strengthened by the solid solution hardening effects of Al, Sn, Si and Mo and precipitation hardening effects of ordered and coherent phase α_2 (Ti_3Al) and relatively coarser and incoherent phase of $(Ti,Zr)_5Si_5$ type silicides [1, 2]. The alloy has been developed for service at temperatures up to 600 °C [1] and is being used for a variety of rotating and stationary components of the compressor module of gas turbine aeroengines [2]. The high pressure compressor disc is exposed to temperatures in the range of 250–550 °C. At these temperatures, dynamic strain aging (DSA), a phenomenon resulting from interaction between solute atoms and mobile dislocations, is known to occur in Timetal 834 [3–5]. Work performed by the authors on Timetal 834 has clearly demonstrated the influence of DSA on mechanical properties such as tensile [4, 5], low cycle fatigue [6–8], fatigue crack growth rate [9] and thermomechanical fatigue [10, 11]. In a recent work, the authors have identified using energy filtered transmission electron microscopy that formation of atmosphere around dislocations by carbon and nitrogen is responsible for DSA in a near-α Ti alloy [12]. While the characteristics of different types of serrations in Timetal 834 at the strain rate of order of 10^{-4} s^{-1} were reported in earlier studies [4], regimes of their occurrence in the form of serration maps has not been reported. In general, activation energy (Q) associated with serrated flow is evaluated to understand the role of solute elements for causing DSA. Although there are several methods to evaluate Q, three methods are largely used which are as follows:

(I) Critical strain based McCormick's model [13, 14]: On the basis of the variation of critical strain, ε_c (the value of pre-strain for onset of serrations) with strain rate and temperature, the value of Q can be determined using the equation [10, 11]:

$$\varepsilon_c^{m+\beta} = K\dot{\varepsilon}\exp(Q/RT) \quad (1)$$

Where m and β are the respective exponents in the relations for the variations of vacancy concentration (C_v) and mobile dislocation density (ρ_m) with plastic strain, $\dot{\varepsilon}$ is the strain rate, K is constant, k is Boltzman constant and T is the absolute temperature. The slope of ln ε_c vs. $1/T$ at constant strain rate can be used to evaluate Q as $Q = slope \times (m+\beta) \times k$

(II) Critical strain based intercept method [15]: This method does not involve the use of $m+\beta$. While one can obtain intercepts on the ln (strain rate) axis corresponding to different level of critical strain at different temperatures from ln (strain rate) vs. ln ε_c, a replot of these intercepts values of ln (strain rate) vs $1/T$ yields the value of Q as $Q = slope \times k$

(III) Magnitude of serration based stress drop method [16]: Alternatively, Q can be evaluated using stress decrements, $\Delta\sigma$ as per the following equation [13]:

$$Q = -R\left[\frac{\Delta \ln \dot{\varepsilon}}{\Delta 1/T}\right]_{\Delta\sigma,\varepsilon} \quad (2)$$

where R is the gas constant.

The aims of the present study are (a) to present the serration map of Timetal 834 over a range of temperature and strain rate, (b) to evaluate the activation energy of DSA using methods I through III mentioned earlier, and (c) to understand the role of Si by comparing the serration map as well as activation energy of Timetal 834 and a near α Ti alloy having similar chemical composition but without Si.

2. Experimental procedure

The nominal chemical composition of the near α Timetal 834 titanium alloy is 5.81 Al – 4.1 Sn –3.71 Zr – 0.74 Nb – 0.53 Mo – 0.35 Si – 0.067 C – 0.09 O – 0.008 N, all in

wt.%. Thick plates of 18 mm of Timetal 834 were solution treated (ST) in α + β region at 1 025 °C (β – transus temperature ~ 1 045 °C) for 2 h followed by oil quenching. The solution heat-treated plates were subjected to a stabilization treatment at 700 °C for 2 hrs before air cooling to room temperature. Alloy 834 near-α Ti-alloy without Si (5.80 Al – 3.9 Sn – 3.68 Zr – 0.73 Nb – 0.54 Mo – 0.068 C – 0.09 O – 0.007 N, all in wt.%), as described in detail in our previous study [12], was used in the present investigation. Henceforth these alloys will be referred as Timetal 834 and Alloy 834, respectively, in the text.

Tensile tests were conducted on round threaded specimens of gauge diameter 4 mm and gauge length 25 mm as per ASTM standard E 8 M [17]. These tests were conducted in an electromechanical test system (Model: Walter + Bai AG) of 200 kN capacity equipped with resistance type three zone split furnace at constant cross-head speeds. Tensile tests were carried out at constant cross-head speeds of 0.01, 0.1, 1, and 10 mm min^{-1}, which correspond to engineering strain rates of 6.67×10^{-6}, 6.67×10^{-5}, 6.67×10^{-4}, and 6.67×10^{-3} s^{-1}, respectively. These tests were carried out at elevated temperatures ranging from 300 °C to 600 °C at an interval of 50 °C. However, additional tests were carried out at 375, 425 and 475 °C. K type thermocouples were used to monitor the temperature during the tests. All tests were started after soaking the specimen for 30 min at the test temperature. A 25 mm gauge length and ± 2.5 mm travel extensometer was used to record the strain during the tests. Three specimens were tested at each test condition. Tensile properties of alloy 834 were evaluated employing the same strain rates and temperature range as that of Timetal 834. However, an additional tensile test was conducted at 250 °C.

3. Results

3.1. Microstructure

The heat treated microstructure of both the alloys as observed is shown in Fig. 1. Timetal 834 as well as alloy 834 shows a bi-modal microstructure which consists of equiaxed primary α in the transformed β matrix. The average size of primary α and prior β grain size was found to be ~ 10 μm and ~ 40 μm, respectively in Timetal 834 (Fig. 1a). The volume fraction of primary α was estimated to be ~ 15 %. The average size of primary α and prior β grain size was found to be ~ 14 μm and ~ 58 μm, respectively in alloy 834 (Fig. 1b). The volume fraction of primary α was estimated to be ~ 17 %. In both the alloys, transformed β grains consist of several secondary α (α_S) colonies, each colony containing alternate laths of secondary α and fine retained β.

3.2. Serrated flow

The plastic regions of true stress–strain curves at various temperatures at a strain rate of 6.67×10^{-4} s^{-1} of both the alloys are shown in Fig. 2. This region clearly shows the load drops or serrated flow in the intermediate temperature range. The plastic region is observed to be smooth at 300, 350 and 500 °C (Fig. 2a) in Timetal 834 while it is smooth at 250 °C and 500 °C in alloy 834. The different types of serrations were labeled following the generally accepted nomenclature in open literature [14] and are shown in Fig. 2c. Type *A* serrations are periodic serrations from repeated deformation bands initiating at the same end of the specimen and propagating in the same direction along the gauge length [14]. These are considered as locking serrations, characterized by an abrupt rise followed by a drop to below the general level of stress–strain curve. They occur in the low temperature part of the DSA regime. Type *B* serrations are oscillations about the general level of the stress–strain curve that occur in the quick succession due to discontinuous band propagation arising from the DSA of the moving dislocations within the band. Type *B* serrations often develop from those of type *A* with increasing strain or occur at the onset of serrated yielding at high temperatures and low strain rates. Type *C* serrations are yield drop that occur below the general level of the flow curve and are therefore considered to be due to dislocation unlocking. They occur at higher temperatures and lower strain rates than in the case of types of *A* and *B* serrations [14].

In the present study, periodic *A* type serrations are observed at 400 °C which were found to change over to type *E* serrations at large strains at 375 °C and 400 °C. At 425 °C, prominent type *B* serrations were noticed, inter-

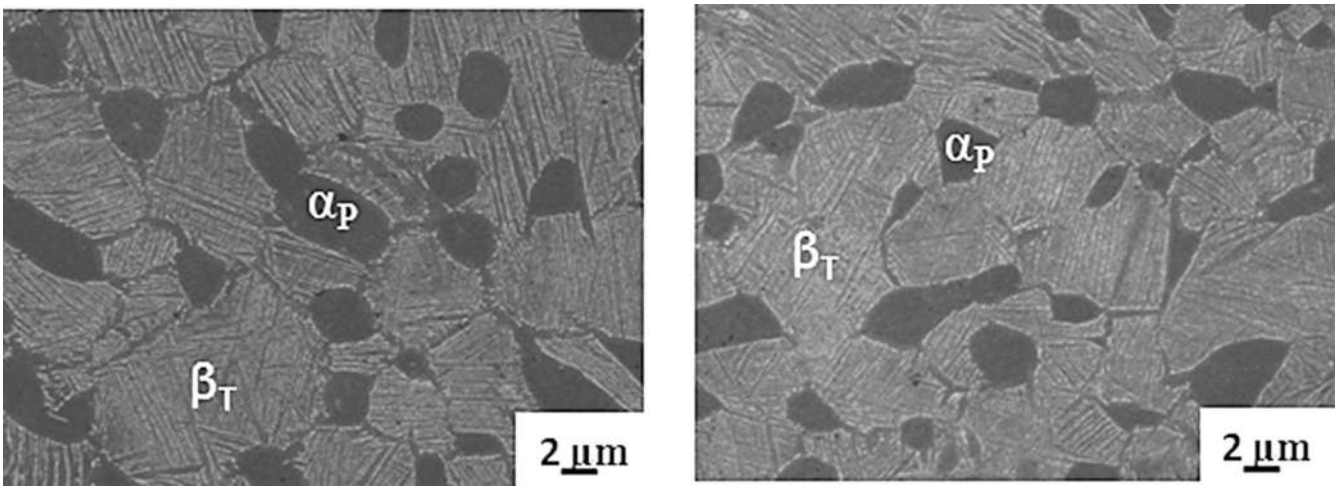

Fig. 1. SEM micrographs of (a) Timetal 834, and (b) alloy 834 without Si showing equiaxed primary α and transformed β matrix.

spersed with few types *A* peaks. At 450 °C and 475 °C, unlocking type *C* serrations were observed. Type *C* serrations were accompanied by type *B* serrations at 450 °C. In alloy 834, serrations of *A* type at 300 °C and 350 °C, *C* type at 400 °C and *C* + *A* type at 450 °C was observed in flow curves (Fig. 2b). It can also be inferred, qualitatively, from Fig. 2a and b that the tendency of strain hardening (increase in stress with respect to increase in strain) is higher in Timetal 834 as compared to alloy 834. A summary of the observations made on serrated flow behavior in form of "serrations maps" for both the alloys are shown in Fig. 3. It is clear from Fig. 3 that the temperature at which DSA is noticed is different for different alloys. The temperature range at which DSA is seen is relatively higher in alloy 834 as compared to Timetal 834 and the characteristics of types of serrations are also different in both the alloys.

3.3. Tensile properties

The variation of tensile properties such as 0.2 % yield strength, ultimate tensile strength (*UTS*), % total elongation and strain hardening exponent as a function of temperature for both the alloys are shown in Fig. 4. It can be seen in Fig. 4a and b that Timetal 834 shows higher strength levels (0.2 % *YS* and *UTS*) as compared to alloy 834. The alloys show similar trends in the variation of strength parameters (0.2 % *YS* and *UTS*) with increase in temperature, i. e. an initial rapid decrease in strength up to certain temperature followed by a plateau and then again rapid decrease in strength with increase in temperature. It is also evident from Fig. 4a and b that the intermediate temperature range up to which the strength remains nearly same, i. e. the region of plateau is relatively wider in alloy 834 as compared to Timetal 834. The alloys show similar trends in the variation of ductility (% total elongation) and strain hardening exponent.

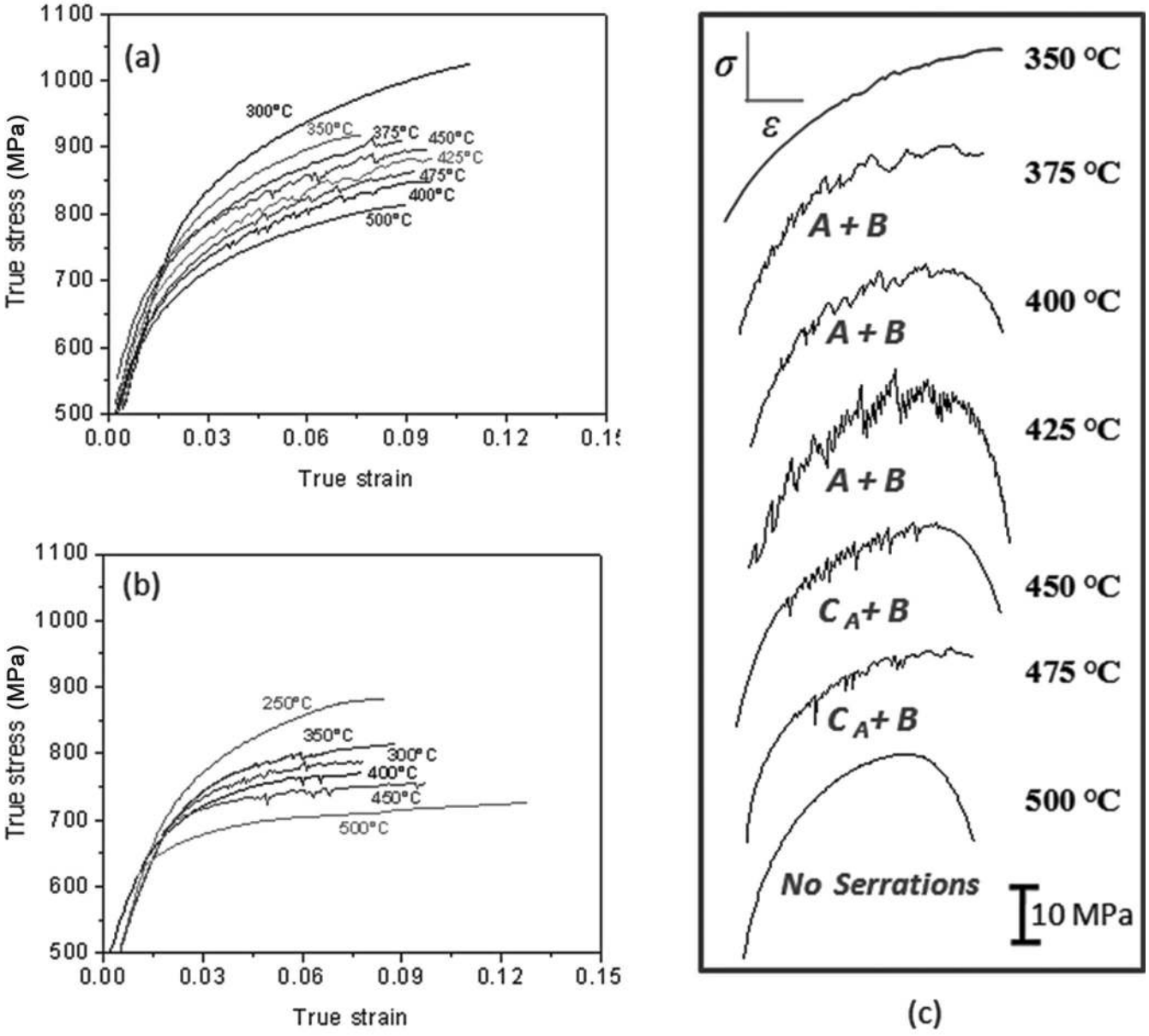

Fig. 2. Plastic region of true stress (MPa) – strain curves of: (a) Timetal 834, and (b) alloy 834 tested at a strain rate of 6.67×10^{-4} s^{-1}. Various types of serrations manifested in Timetal 834 are shown in (c).

While Timetal 834 exhibits minimum ductility (Fig. 4c) and maximum strain hardening exponent (Fig. 4e) at 450 °C, similar behavior was observed at 350 °C in alloy 834 (Fig. 4d and f).

Strain rate jump (SRJ) tests were conducted to analyze the strain rate sensitivity of both alloys [15]. These tests were conducted at the beginning of plastic deformation, i. e. at a small plastic strain of $\varepsilon_p = 0.02$. The representative stress–strain curves corresponding to occurrence of serrations (450 °C) and non-occurrence of serrations (300 °C) obtained during SRJ tests of Timetal 834 are shown in Fig. 5a and b, respectively. It is evident that a sudden decrease in strain rate leads to increase in stress at 450 °C (Fig. 5a), whereas a sudden increase in strain rate leads to increase in stress at 300 °C (Fig. 5b).

The stress increment ($\Delta\sigma$) which occurs immediately after the strain rate jump has been estimated by means of extrapolation as indicated in these figures. The strain rate sensitivity (m) is evaluated through the relation [18]:

$$m = \frac{d\sigma}{d \ln \dot{\varepsilon}} \cong \frac{\Delta\sigma}{\Delta \ln \dot{\varepsilon}} \quad (3)$$

The variation of m with temperature for both the alloys is shown in Fig. 6. While m values are positive at 300, 350, 500 and 600 °C where the flow curves are smooth, it is negative at 375, 400, 425, 450 and 475 °C where serrated flow is observed in Timetal 834 alloy (Fig. 6a). In the case of alloy 834, m values are negative at 300, 350, 400, 450, and 500 °C, whereas, they are positive at 250, 550 and 600 °C (Fig. 6b).

3.4. Determination of activation energy

It is evident from Fig. 2a and b that serrated yielding commenced at a well defined plastic strain level. The critical true plastic strain, ε_c was evaluated from the true stress–strain curves as the minimum true plastic strain at which a perceptible load drop of 5 N occurs. The variation of ε_c as a function of strain rate at 400, 450 and 475 °C in Timetal 834 is shown in Fig. 7a. The same plot for alloy 834 at 300, 350, 400, 450 and 500 °C is shown in Fig. 7b. It is evident from Fig. 7b that the variation of ε_c with strain rate follow a systematic trend at all test temperatures in alloy 834. The same trend has been observed in Timetal 834 at

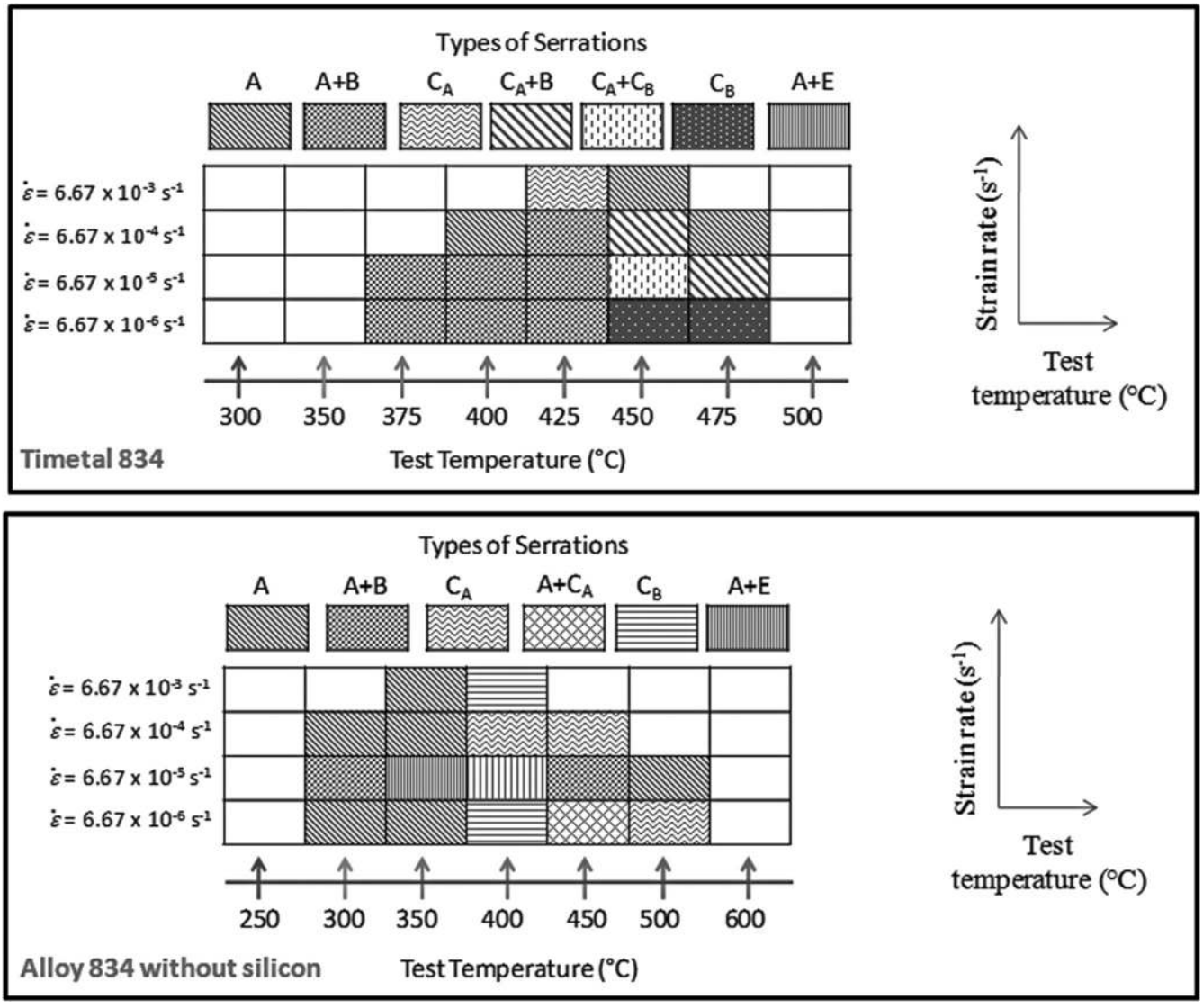

Fig. 3. The schematic classification of serrations as a function of temperature and strain rate for: (a) Timetal 834, and (b) alloy 834 without silicon.

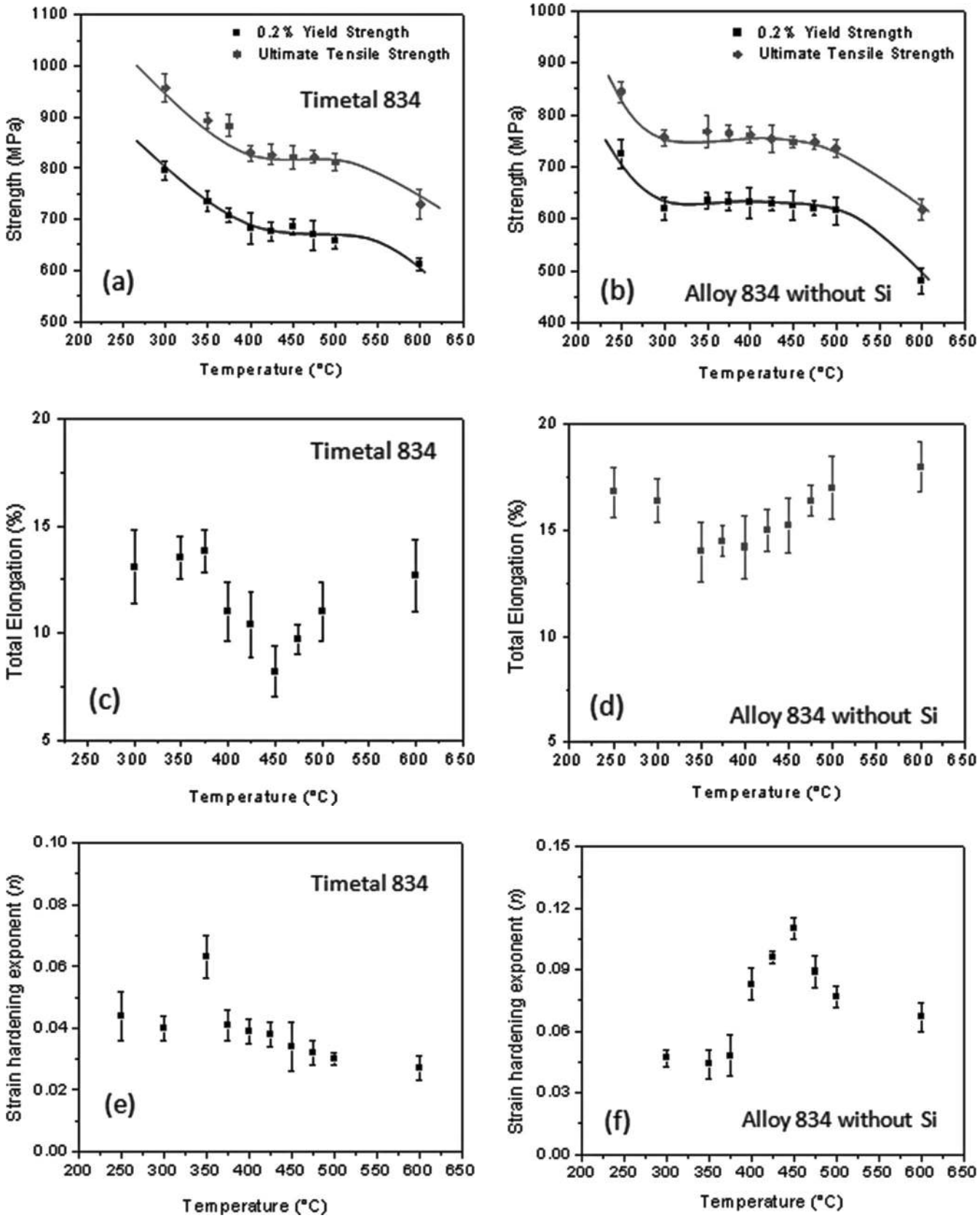

Fig. 4. Influence of temperature on: (a, b) 0.2% yield strength (MPa) and tensile strength (MPa), (c, d) % total elongation, and (e, f) strain hardening exponent of Timetal 834 (a, c, e) and alloy 834 without Si (b, d, f).

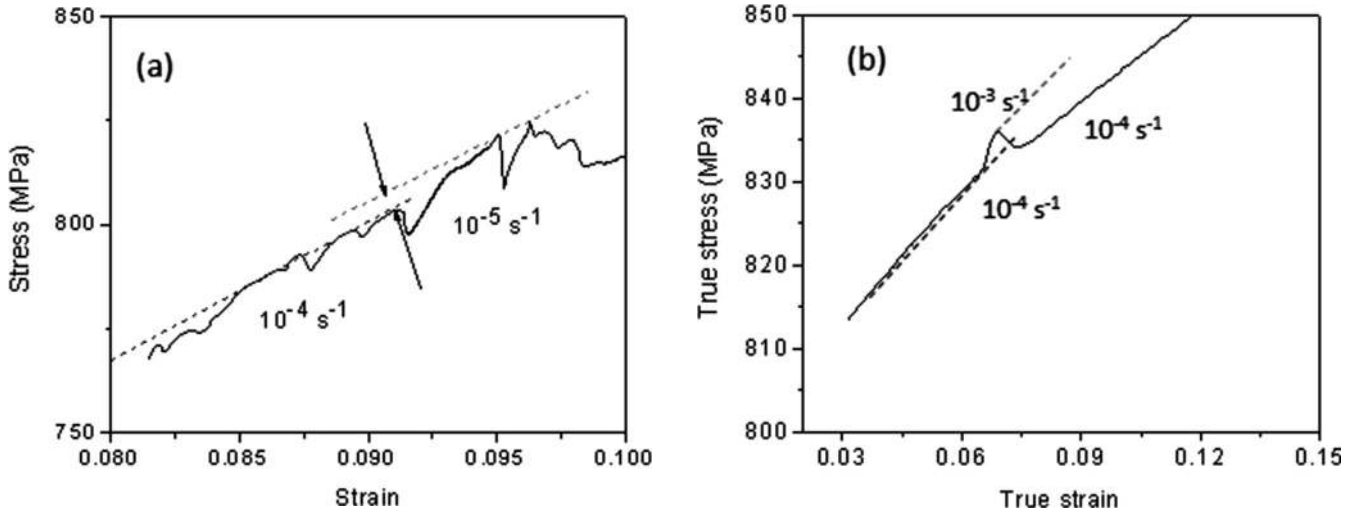

Fig. 5. Nature of transients during strain rate jump tests at: (a) 450 °C, serrated region, and (b) 300 °C, non-serrated region of Timetal 834.

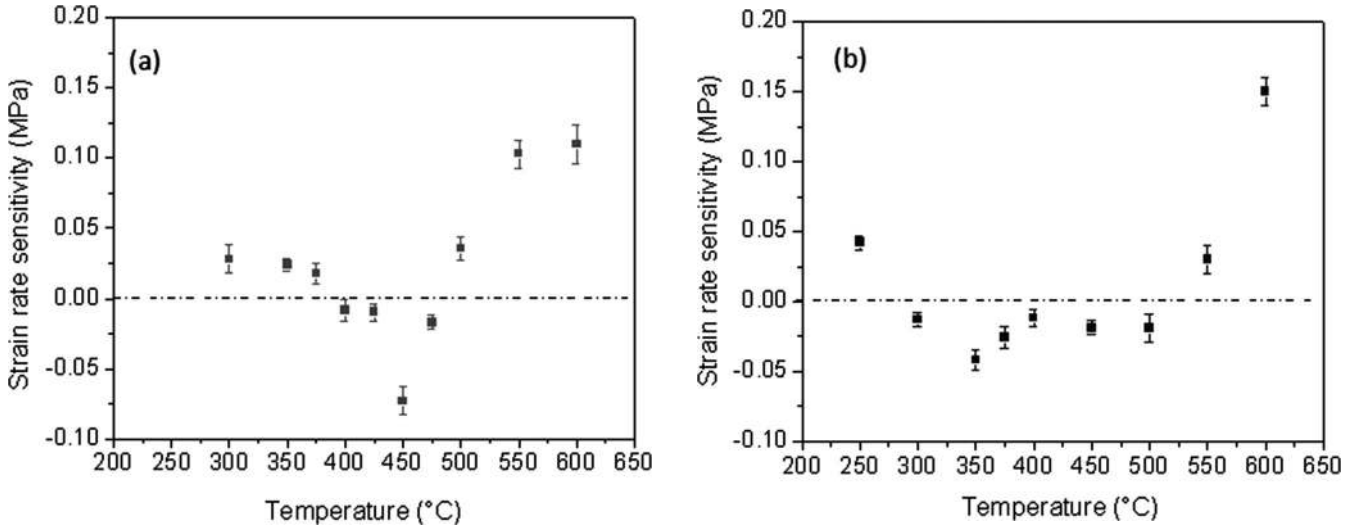

Fig. 6. Variation of strain rate sensitivity as a function of temperature of: (a) Timetal 834, and (b) alloy 834 without Si.

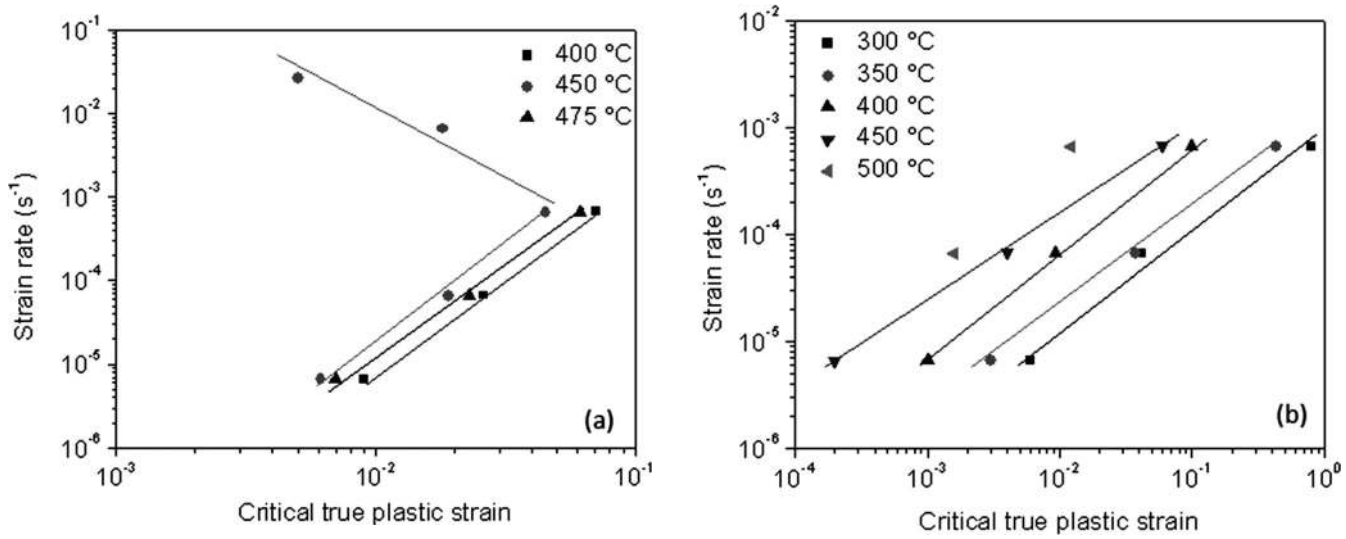

Fig. 7. Variation of critical true plastic strain with strain rate for the onset of serrations in: (a) Timetal 834, and (b) alloy 834.

400 °C and 475 °C, however, ε_c initially increased with increasing strain rate up to 6.67×10^{-4} s^{-1}, beyond which it decreased with increasing strain rate at 450 °C. The values of $m + \beta$ were determined using the positive slopes of Fig. 7a and b. These values are listed in Table 1 and are used for determining activation energy (Q) as per method (I) as outlined in Section 1. The average Q value obtained using this method is 109 kJ mol^{-1} for Timetal 834 (Fig. 8). The average value of Q, computed using method (II) and (III) i.e. intercept method (Fig. 9) and stress drop method (Fig. 10) are found to be 105 kJ mol^{-1} and 84 kJ mol^{-1}, respectively for Timetal 834. The average Q values obtained using critical strain method is 187 kJ mol^{-1} for alloy 834 (Fig. 11). The value of Q computed using stress drop meth-

Table 1. Constant as per vacancy model ($m + \beta$), and activation energy values of lattice diffusion (Q, in kJ mol^{-1}) obtained by critical strain, intercept and stress drop methods for both alloys.

Temperature, T (°C): ($m + \beta$)			
Timetal 834	400 : (2.23)	450 : (2.29)	475 : (2.12)
	Average $m + \beta$ value: 2.21		
Methodology	Activation energy, Q (kJ mol^{-1}) : (strain rate/critical strain/stress drop)		
(I) Critical strain	110 : (6.67×10^{-6} s^{-1})	113 : (6.67×10^{-5} s^{-1}) $Q_{average}$ = 109 kJ mol^{-1}	105 : (6.67×10^{-4} s^{-1})
(II) Intercept	102: (ε_c = 0.08)	111: (ε_c = 0.12) $Q_{average}$ = 105 kJ mol^{-1}	101: (ε_c = 0.22)
(III) Stress drop	77 : ($\Delta\sigma$ = 10 MPa)	90 : ($\Delta\sigma$ = 15 MPa) $Q_{average}$ = 84 kJ mol^{-1}	

Temperature, T (°C) : ($m + \beta$)					
Alloy 834	300 : (0.92)	350 : (0.93)	400 : (0.96)	450 : (0.87)	500 : (-)
	Average $m + \beta$ value : 0.92				
Methodology	Activation energy, Q (kJ mol^{-1}) : (strain rate/critical strain/stress drop)				
(I) Critical strain	185.32 : (6.67×10^{-6} s^{-1}) 195.21 : (6.67×10^{-5} s^{-1}) 182.14 : (6.67×10^{-4} s^{-1}) $Q_{average}$ = 187 kJ mol^{-1}				
(III) Stress drop	132 : ($\Delta\sigma$ = 10 MPa)				

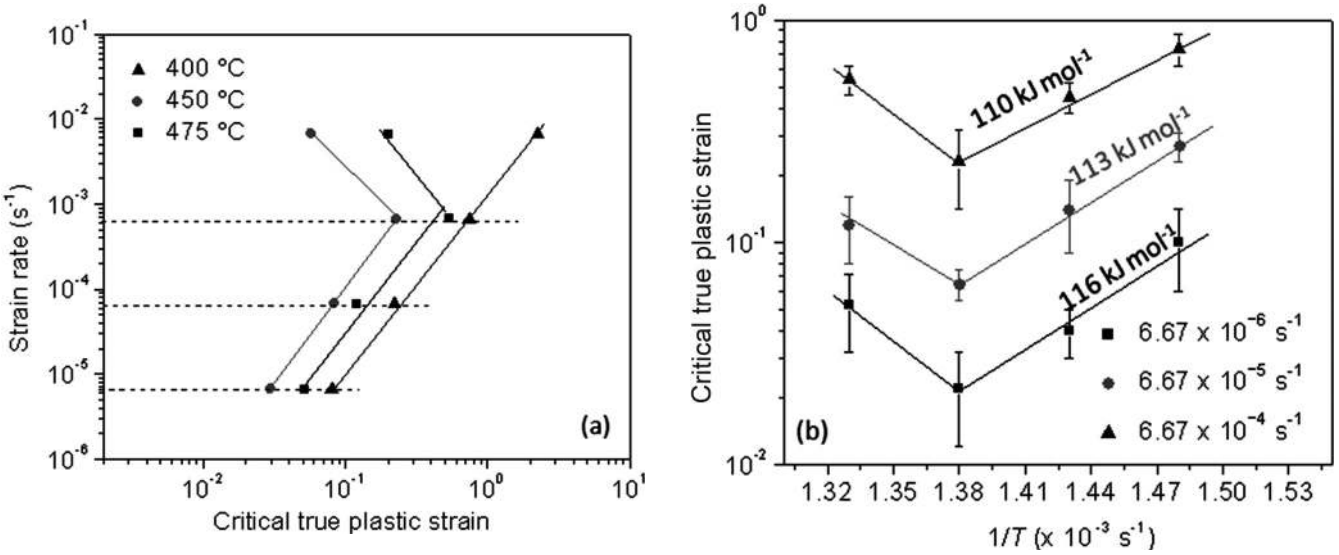

Fig. 8. Plots of (a) ln (strain rate) versus ln (ε_c) at different temperatures, and (b) ln (ε_c) versus 1/T at different strain rates for Timetal 834. The activation energy determined by critical strain method is shown in (b).

od as shown in Fig. 12 yields 132 kJ mol^{-1} for alloy 834. These values of activation energy for both the alloys are listed in Table 1.

4. Discussion

It is clear in this study that the tensile test parameters viz., temperature and strain rate strongly influence the tensile properties viz., 0.2% yield strength (0.2% *YS*), ultimate tensile strength (*UTS*), % total elongation and strain hardening exponent (*n*). The manifestation of serrations in the flow curve (Fig. 2a and b), a plateau in the variation of 0.2% and *UTS* (Fig. 4a and b), a local minimum in the variation of ductility (Fig. 4c and d), a peak in strain hardening exponent (Fig. 4e and f), and negative strain rate sensitivity (Fig. 6) confirm the occurrence of dynamic strain aging [14, 19] in both the alloys.

4.1. Characteristics of dynamic strain aging

While the Portevin–Le Chatelier (PLC) effect is observed to be normal, i.e. increase in ε_c with increasing temperature (Fig. 2) in alloy 834, an inversion from the normal PLC effect at low strain rates to inverse PLC effect at higher strain rate (Fig. 7a) at 450 °C has been observed in Timetal 834. Further, unlocking type *C* serrations were observed at this test temperature in Timetal 834 (Fig. 2a and c). As it is known that Si normally stays in solid solution up to 450 °C and it comes out of solid solution as silicide-type precipitates beyond 450 °C [20], it is likely that silicide precipitation during the test decreased the concentration of Si in the matrix and led to the inverse PLC effect. This further supports the well reported hypothesis that unlocking type serrations during the inverse PLC effect are related to precipitation during the test [21].

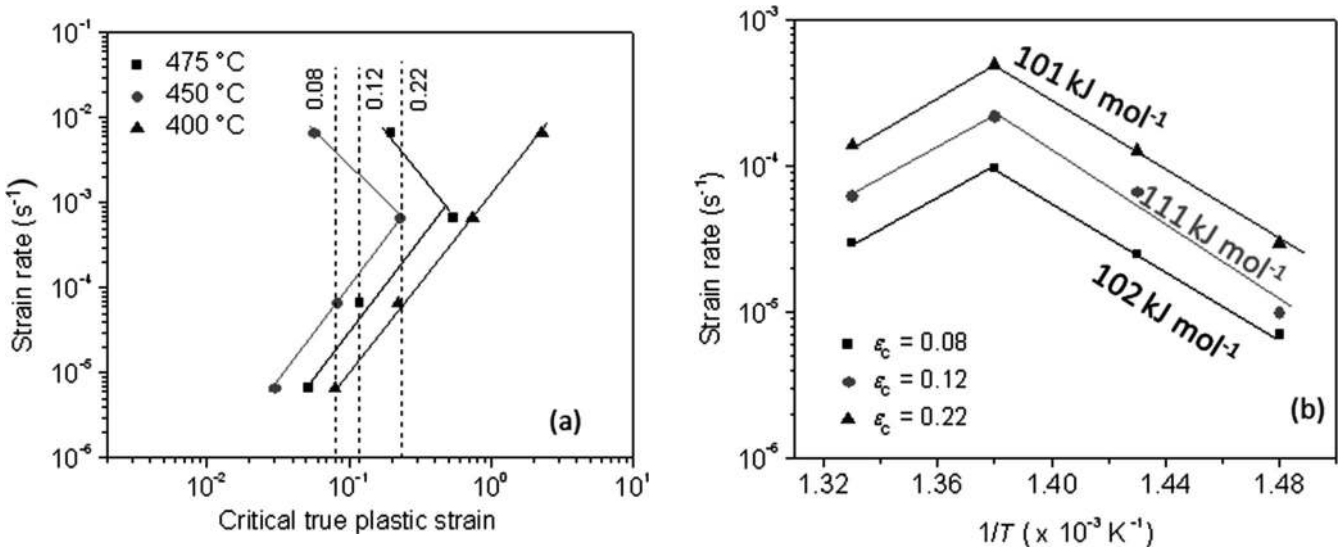

Fig. 9. Plots of (a) ln (strain rate) versus ln (ε_c) at different temperatures, and (b) ln (strain rate) versus 1/*T* at different ε_c in Timetal 834. The activation energy determined by intercept method is shown in (b).

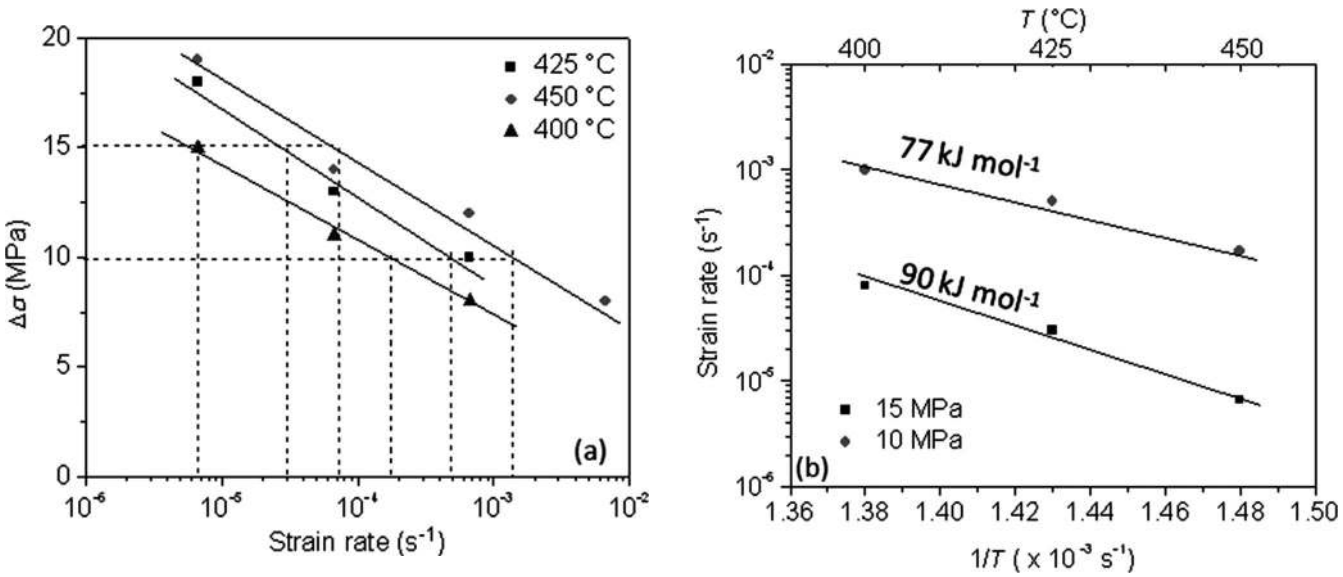

Fig. 10. Plots of (a) $\Delta\sigma$ versus ln (strain rate) at different temperatures, and (b) ln (strain rate) versus 1/*T* at different $\Delta\sigma$ in Timetal 834. The activation energy determined by stress drop method is shown in (b).

As per the vacancy model [22], $m + \beta$ values generally range from 2 to 3 for substitutional alloys and 0.5 to 1 for interstitial alloys. The average $m + \beta$ value (2.21, Table 1) in Timetal 834 indicates locking of dislocations by substitutional solute/solutes, whereas, $m + \beta$ value (0.92, Table 1) in alloy 834 suggests the role of interstitial solute/solutes in immobilizing dislocations. Further, the activation energies for diffusion of substitutional as well as interstitial solute elements in α titanium are listed in Table 2 [23, 24]. It is clear from Table 1 and Table 2 that the average apparent activation energy for serrated flow in Timetal 834 (100 kJ mol^{-1}) matches well with the Q value of diffusion of Si (105 kJ mol^{-1}). This suggests that Si is responsible for DSA effects in Timetal 834. This is further corroborated by the observed $m + \beta$ value (Table 1) indicating a substitutional solute diffusion controlled mechanism of DSA in Timetal 834.

In other hand, the average value of activation energy for serrated flow in alloy 834 (160 kJ mol^{-1}) matches reasonably well with the Q value of substitutional solutes such as Al, Mo, Nb, Zr and also interstitial solute C (Table 2). However, as the $m + \beta$ value (Table 1) corresponds to that for interstitial solute to form the locking atmosphere, it is unlikely that a substitutional solute element plays any role in this process. Moreover, a detailed investigation using energy filtered transmission electron microscopy (EFTEM) on interrupted samples of alloy 834 showed the segregation of carbon (C) and nitrogen (N) to dislocations [12]. The Q values and direct experimental evidence using EFTEM confirms that carbon and nitrogen causes the DSA effect in alloy 834, as described in detail in our previous study [12].

The relatively higher magnitude of serrations and pronounced negative strain rate sensitivity (m) in Timetal 834

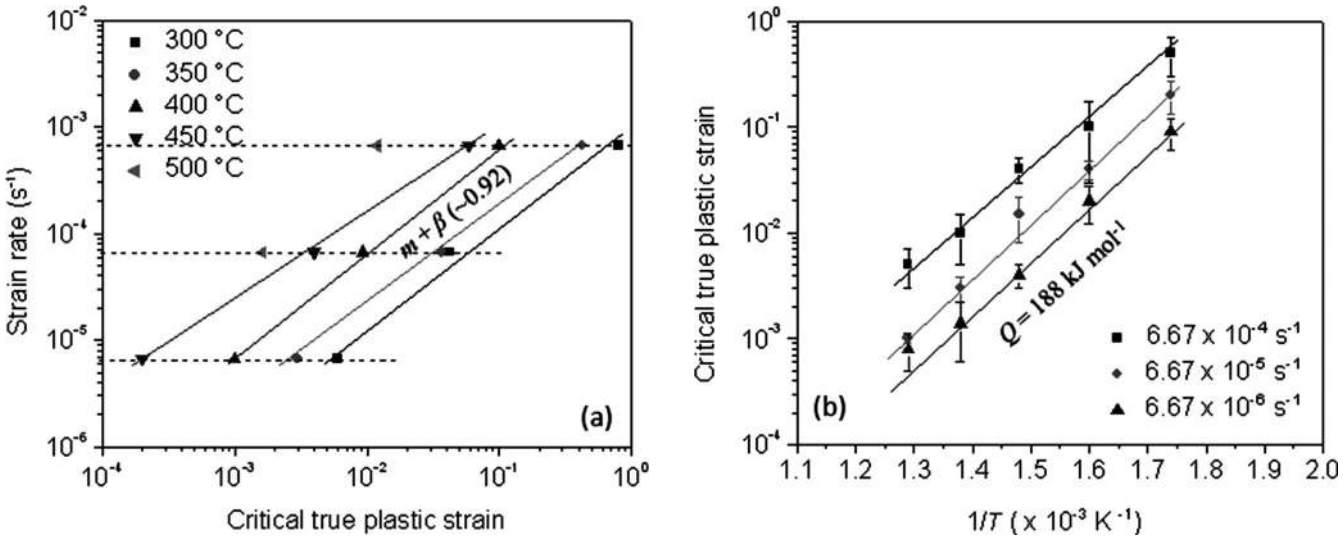

Fig. 11. Plots of (a) log (strain rate) vs log (critical plastic strain), and (b) log (critical plastic strain) vs. reciprocal temperature. The activation energy (kJ mol^{-1}) determined by critical strain method in alloy 834 is shown in (b).

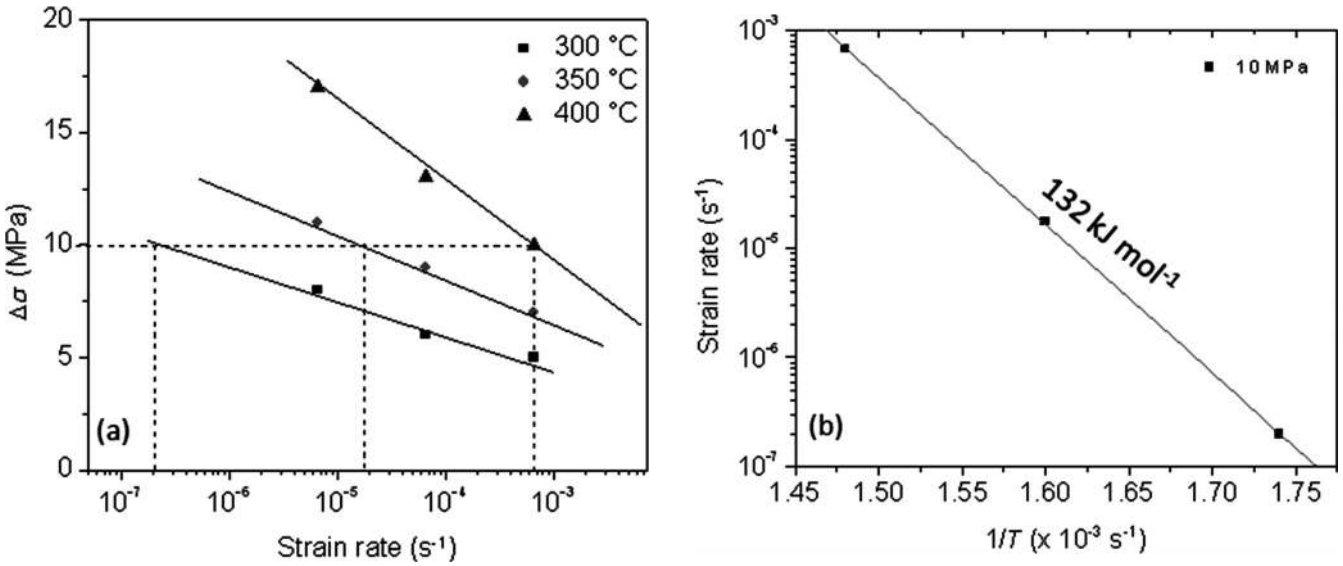

Fig. 12. Plots of (a) $\Delta\sigma$ versus ln (strain rate) at different temperatures, and (b) ln (strain rate) versus $1/T$ at $\Delta\sigma$ = 10 MPa in alloy 834. The activation energy determined by stress drop method in alloy 834 is shown in (b).

Table 2. Activation energy (kJ mol^{-1}) of lattice diffusion of various elements in α-titanium.

Elements	Activation Energy (kJ mol^{-1})
Substitutional	
Al	156
Mo	180
Si	105
Nb	165
Zr	148
Sn	132
Self-diffusion (Ti)	192
Interstitial	
C	182
N	228
O	200

indicates that pinning of dislocations is more effective and stronger in Timetal 834 as compared to alloy 834. Interestingly, this observation is in contrast to the belief that interaction of substitutional solute elements with dislocations is weaker than interstitials and hence, the magnitude of serrations as well as *m* should have been more pronounced in alloy 834 and not in Timetal 834. This anomaly can be explained considering the elastic interaction energy due to both size and modulus effect [18]. As originally envisaged by Winstone et al. [25], the presence of a substitutional–interstitial complex leads to more effective interaction between both edge and screw components of dislocations. Based on this hypothesis, it is reasonable to conclude that in the case of Timetal 834, the presence of an Si–C–N complex leads to more effective interaction between both edge and screw components of dislocations. In isolation either an interstitial or a substitutional atom alone is not expected to be very effective. However, this needs to be viewed in light of direct experimental evidence and is outside the scope of the present investigation. Similar to that of bcc metals, the occupancy of interstitial/octahedral sites in the hcp lattice by interstitial solute elements leads to a strong tetragonal distortion of the lattice [26]. In this case, it is possible for both screw and edge dislocations to interact with the Si–C–N complex pairs and hence the "Si–C–N" complex can be considered to act as "hard" obstacles to dislocation glide in Timetal 834. In addition, considering the modulus effect, Si is a "softer" substitutional solute atom as compared to titanium as a solvent atom and hence it attracts more dislocations to interact in the solid solution. In other words, the self energy of dislocations with Si-interstitial solutes complex surrounding it is less in Timetal 834 than in the alloy 834. This approach suggests that Si has the ability to enhance the effectiveness of the DSA effect caused by carbon and nitrogen as interstitial elements. Detailed separate investigations on Timetal 834 alloys with and without interstitial elements is necessary to unambiguously prove this hypothesis of effectiveness of Si-interstitial complex on enhancing the magnitude of serrations and is the scope of future investigations.

5. Conclusions

Effects of Si, considering Timetal 834 with Si and alloy 834 without Si, on the characteristics of dynamic strain aging have been examined. The tensile properties have been evaluated as a function of both strain rate (10^{-6} to 10^{-3} s^{-1}) and temperature (250 – 600 °C). The following major conclusions can be drawn from this study:

1. Silicon as a substitutional solute has the ability to enhance the effects of dynamic strain aging (DSA) caused by carbon and nitrogen as interstitial solutes in Timetal 834. Silicon addition raises the temperature for the onset of DSA.
2. It is proposed that Si enhances the effectiveness of DSA through size and modulus effects. While pairs of silicon-interstitial atoms are believed to act as hard obstacles to dislocation glide, presence of silicon decreases the self energy of dislocations for effective dislocation–solute interaction.

The authors thank Director, DMRL for his encouragement in this research activity. The authors would like to acknowledge the support of Shri G B Vikram for the help in carrying out tensile testing. The authors are grateful to Defence Research and Development Organization for providing the funding and facilities to carry out this work.

References

[1] D.F. Neal, in: P. Lacombe, R. Tricot, G. Beranger (Eds.), Proc. 6th World Conference on Titanium, Cannes, France (1988) 253 – 258.
[2] G. Lütjering, J.C. Williams: Titanium, 2nd Ed., Springer, Berlin (2007).
[3] N. Singh, V. Singh: Metall. Mater. Trans. A 30 (1999) 2547. DOI:10.1007/s11661-999-0263-x
[4] K. Prasad, V.K. Varma: Mater. Sci. Eng. A 486 (2008) 158. DOI:10.1016/j.msea.2007.09.020
[5] K. Prasad, S.V. Kamat: Mater. Sci. Eng. A 490 (2008) 477. DOI:10.1016/j.msea.2008.01.005
[6] K. Prasad, R. Sarkar, P. Ghosal, V.K. Varma: Mater. Sci. Eng. A 494 (2008) 227. DOI:10.1016/j.msea.2008.04.025
[7] K. Prasad, V. Kumar: Mater. Des. 31 (2010) 2716. DOI:10.1016/j.matdes.2010.01.031
[8] K. Prasad, R. Sarkar, V. Kumar, K.B.S. Rao, M. Sundararaman: Mater. Sci. Eng. A 662 (2016) 373. DOI:10.1016/j.msea.2016.03.079
[9] K. Prasad, S. Abhaya, G. Amarendra, V. Kumar, K.V. Rajulapati, K.B.S. Rao: Eng. Fract. Mech. 102 (2013) 194. DOI:10.1016/j.engfracmech.2013.02.017
[10] K. Prasad, V. Kumar, K.B.S. Rao, M. Sundararaman: Metall. Mater. Trans. A 47 (2016) 3713. DOI:10.1007/s11661-016-3482-y
[11] K. Prasad, R. Sarkar, K.B.S. Rao, M. Sundararaman: Metall. Mater. Trans. A 47 (2016) 4904. DOI:10.1007/s11661-016-3670-9
[12] K. Prasad, S. Amrithapandian, B.K. Panigrahi, V. Kumar, K.B.S. Rao, M. Sundararaman: Mater. Sci. Eng. A 638 (2015) 90. DOI:10.1016/j.msea.2015.04.060
[13] P.G. McCormick: Acta Metall. 20 (1972) 351. DOI:10.1016/0001-6160(72)90028-4
[14] P. Rodriguez: Bull. Mater. Sci. 6 (1984) 653. DOI:10.1007/BF02743993
[15] K.W. Qian, R.E. Reed-Hill: Acta Metall. 31 (1983) 87. DOI:10.1016/0001-6160(83)90067-6
[16] E. Pink, A. Grinberg: Acta Metall. 30 (1982) 2153. DOI:10.1016/0001-6160(82)90136-5
[17] ASTM Standard E 8/8M-11: Standard test methods for tension testing of metallic materials. In: Annual book of ASTM standards, vol. 3.01, ASTM International, West Conshohocken (PA), USA (2012).
[18] G.E. Dieter: Mechanical Metallurgy, McGraw-Hill Book Co., London, UK (1988).

[19] J.M. Robinson, M.P. Shaw: Int. Mater. Rev. 39 (1994) 113. DOI:10.1179/imr.1994.39.3.113
[20] D.F. Neal, S.P Fox, in: F.H. Froes, I. Caplan (Eds.), Titanium 92 Science and Technology, The Minerals, Metals & Materials Society (1993) 287–294.
[21] R.W. Hayes, W.C. Hayes: Acta Metall. 32 (1984) 259. DOI:10.1016/0001-6160(84)90054-3
[22] V.D. Beukel: Acta Metall. 28 (1980) 965. DOI:10.1016/0001-6160(80)90114-5
[23] M. Doner, H. Conrad: Metall. Trans. 4 (1973) 2809. DOI:10.1007/BF02644581
[24] H. Conrad: Prog. Mater. Sci. 26 (1981) 123. DOI:10.1016/0079-6425(81)9001-3
[25] M.R. Winstone, R.D. Rawlings, D.R.F. West: J. Less Common Metals 31 (1973) 143. DOI:10.1016/0022-5088(73)90137-9
[26] R.E. Smallman, R.J. Bishop: Modern Physical Metallurgy and Materials Engineering, 6th Ed., Butterworth Heinemann, UK (1999) 219.

(Received June 21, 2016; accepted November 29, 2016; online since February 2, 2017)

Correspondence address

Kartik Prasad, PhD
Scientist, Mechanical Behavior Group
Defence Metallurgical Research Laboratory
Kanchanbagh
Hyderabad – 500 058
India
Tel.: +91 40 24586407
Fax: +91 40 24340266
E-mail: kartik@dmrl.drdo.in

Bibliography
DOI 10.3139/146.111478
Int. J. Mater. Res. (formerly Z. Metallkd.)
108 (2017) 4; page 275–285

ISSN 1862-5282